Published in *Engineering Turbulence Modelling and Experiments - 5*
edited by W. Rodi & N. Fueyo (Elsevier, 2002), pp. 607-616

ACTIVE CONTROL FOR DRAG REDUCTION IN TURBULENT PIPE FLOW

Koji Fukagata [1, 2] and Nobuhide Kasagi [1]

[1] Department of Mechanical Engineering, The University of Tokyo
7-3-1 Hongo, Bunkyo-ku, Tokyo 113-8656, Japan
[2] Institute for Energy Utilization, AIST
1-2-1 Namiki, Tsukuba-shi, Ibaraki 305-8564, Japan

ABSTRACT

Active control of turbulent pipe flow is studied by means of direct numerical simulation (DNS). First, the active cancellation control proposed by Choi et al. (1994) is tested in the DNS of turbulent pipe flow at $Re_b = 3050$ and 5300, which is based on the bulk-mean velocity and the pipe diameter. The drag reduction rate attained by this control is found to be almost the same as in the case of turbulent channel flow, i.e., about 20 %. Then, the control is applied only partially over a limited length in the streamwise direction, but not on the entire wall surface. The upstream control effect remains over a distance of about $2000 - 2500$ wall units downstream of the point where the control is terminated; the mechanism of this relatively rapid deterioration is examined by analyzing the turbulent stress budget.

KEYWORDS

Pipe flow, Turbulence control, Drag reduction, Direct numerical simulation, Active cancellation, Partial wall surface, Budget.

INTRODUCTION

During the last decade, so-called active feedback control of turbulent flow has attracted much attention. Its application is diverse, e.g., reduction of skin frictional drag of long-distance gas/petroleum pipelines and large-scale ships, enhancement of mixing in heat exchangers and bio-reactors, and noise reduction of high-speed vehicles.

An active feedback control system generally consists of three functional hardware components as shown in Figure 1, i.e., sensors, controllers and actuators, and an additional software component, i.e., a control algorithm which determines the action of actuators depending upon the sensor output. In parallel with intensive R&D studies of hardware components, the control algorithm has been mainly

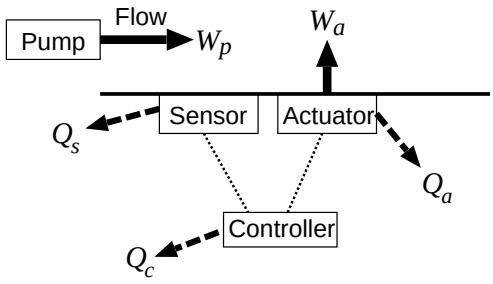

Figure 1 : Schematic of the active-feedback control system.

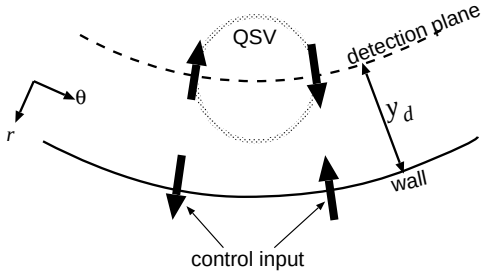

Figure 2 : Active cancellation control in pipe.

developed and assessed by using direct numerical simulation (DNS) of controlled turbulent flow fields.

Choi et al. (1994) attained considerable drag reduction in their DNS of turbulent channel flow by local wall blowing and suction, of which velocity, v_w, is determined so as to oppose the velocity components induced by the near-wall quasi-streamwise vortices (QSVs). Their study assumed a highly idealized situation with the use of a virtual detection plane in the flow and by blowing and suction continuously distributed over a wall surface at low Reynolds numbers. However, later efforts were devoted to the study of this control algorithm for a more realistic control system, e.g., sensing on the wall surface instead of assuming a virtual detection plane (Lee et al., 1998), the use of discrete wall-deformation actuators instead of spatially continuous blowing and suction (Endo et al., 2000) [1], and control at higher Reynolds numbers (Iwamoto et al., 2002). These studies demonstrated that the above active cancellation strategy proposed by Choi et al. (1994) should be effective even for the drag reduction in more practical situations.

Most of the previous studies have dealt with plane channel flows, while a flow in a circular pipe is another canonical wall-bounded flow and its control has several direct practical applications. Control of pipe flow by rotation (Orlandi & Fatica, 1997) and by oscillation around its axis (Quadrio & Sibilla, 2000) has been reported with some degree of success. However, more widely applicable wall actuation control mentioned above should be tested in pipe flows. It would also be interesting to explore if the control algorithm proposed for channel flow is also valid for pipe flow. Therefore, in the first part of the present study, an active control algorithm is applied to a turbulent pipe flow. Here, we mainly focus on the overall control performance and provide data useful for a feasibility study of real control systems.

In reality, it may not be possible both technologically and financially to have an entire wall surface equipped with an array of active feedback control units. In many perspective cases, the number of actuators / sensors should be limited. In the previous DNS studies, however, the control has always been assumed on the entire surface, so that the knowledge on spatially inhomogeneous control is lacking. The second part of the present study is therefore devoted to a control only applied on a limited wall surface area. DNS is carried out by dividing the computational domain into two and the control is applied only in the upstream sub-region of a pipe.

The paper is organized as follows. The numerical method and control algorithm used are briefly described in the next section. Computational results are presented and discussions are made for the basic case and for the cases of control on partial wall surface in subsequent two sections. Finally, in the last section, conclusions are derived.

NUMERICAL METHOD

A computational code for DNS of turbulent pipe flow was developed based on a second-order accurate finite difference scheme on the cylindrical coordinate system. A special care was paid for consistency in the discretized space so that the energy is conserved by the inviscid part of the governing equation

[1] Reference has been corrected from the published version

TABLE 1
COMPUTATIONAL CONDITIONS.

Re_b	$Re_{\tau u}$	L_z/R	L_z^+	N_r	N_θ	N_z	Δr^+	$(R\Delta\theta)^+$	Δz^+
3050	110	35	3850	64	128	256	0.43 - 2.74	5.40	15.04
5300	184	40	7360	48	128	512	0.95 - 6.11	8.84	14.06

(Fukagata & Kasagi, 2002). The time integration was advanced by using the third order accurate Runge-Kutta / Crank-Nicolson (RK3/CN) scheme, which was similar to that used by Rai & Moin (1991). The statistics of an uncontrolled flow at $Re_\tau = u_\tau R/\nu = 180$ ($Re_b = 2U_b R/\nu \simeq 5300$) computed by using the present code were in excellent agreement with previous DNS data by Eggels et al. (1994).

Throughout the present work, the mass flow rate, i.e., the bulk mean velocity U_b was kept constant. For that purpose, a modified fractional method (You et al., 2000) was adopted as a time splitting method. A fully developed turbulent flow is assumed in a circular pipe of a radius R, but the computation is made in a pipe of finite length L with periodic boundary conditions at both ends. Thus, strictly speaking, the flow field should be always periodic in the streamwise direction, and it is particularly so in the case of partial area control. The size of computational domain and computational mesh used are shown in Table 1. Hereafter, superscript $+$ is used for the dimensionless quantity normalized by the friction velocity of uncontrolled flow and the kinematic viscosity.

The control algorithm used in the present study is so-called active cancellation control (v-control) of Choi et al. (1994), i.e.,

$$v_w = -u_r(y_d)\ . \tag{1}$$

Here, y_d denotes the distance between wall and a virtual detection plane as shown in Figure 2, and v_w is the radial velocity at the wall, i.e., $v_w = u_r|_{r=R}$.

CONTROL ON ENTIRE WALL

The investigation is initiated with active cancellation control applied on the entire wall with different locations of the detection plane, $y_d^+ = (R-r)^+$. Simulations were performed for two relatively low Reynolds numbers, $Re_b = 3050$ ($Re_{\tau u} \simeq 110$) and $Re_b = 5300$ ($Re_{\tau u} \simeq 180$). Note that, in the case of $Re_b = 3050$, low-frequency intermittency was observed which suggested that the flow remained in a transitional slug flow region.

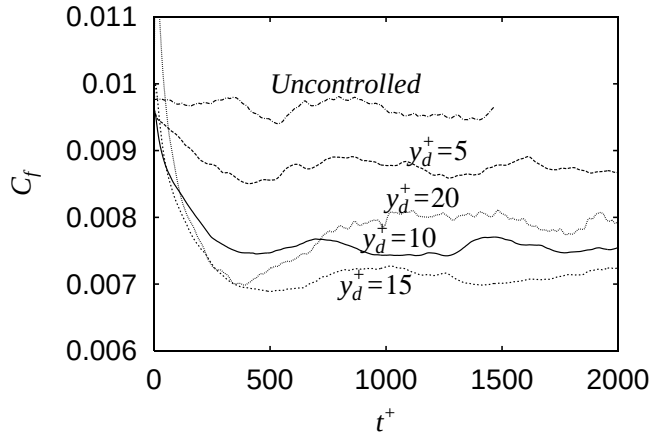

Figure 3: Time trace of the skin friction coefficient ($Re_b = 5300$).

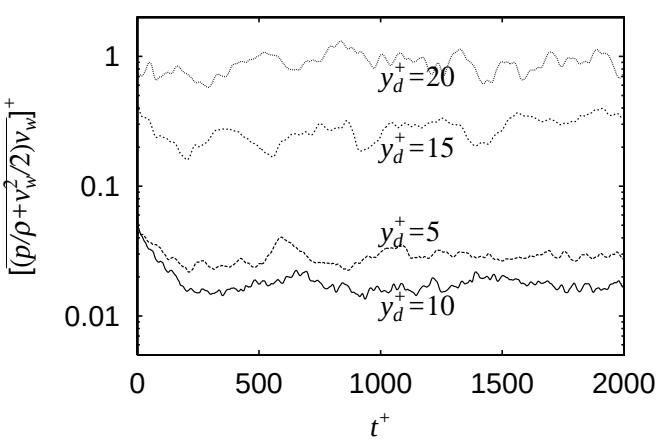

Figure 4 : Time trace of the power input ($Re_b = 5300$).

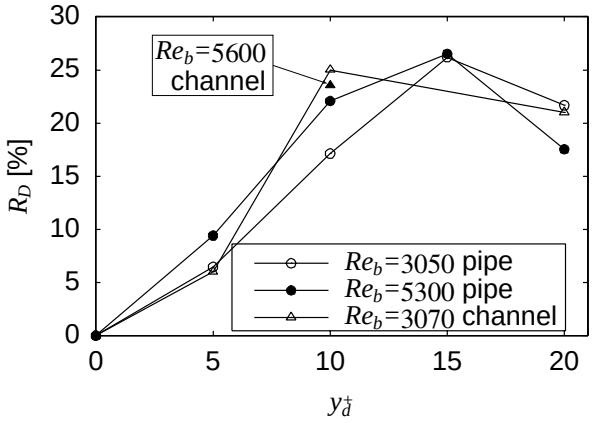

Figure 5: Drag reduction rate, R_D.

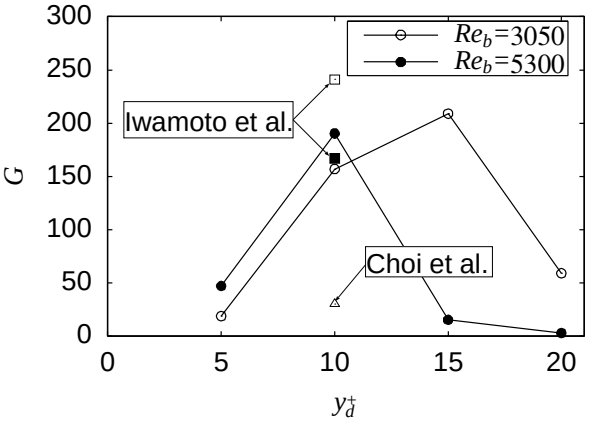

Figure 6 : Control gain, G.

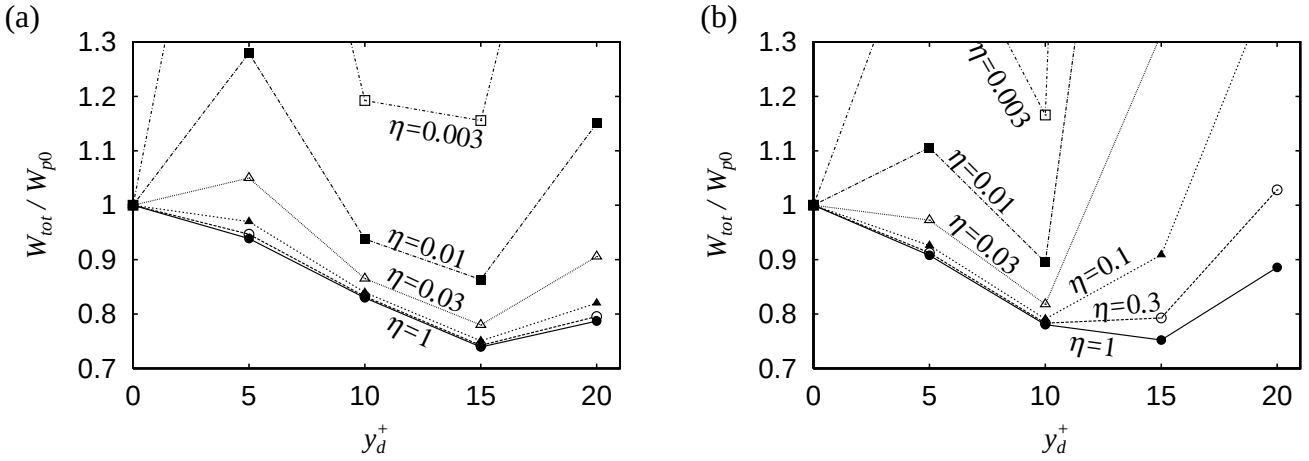

Figure 7 : Total power saving ratio with different system hardware efficiency. (a) $Re_b = 3050$; (b) $Re_b = 5300$.

The simulation was started from a fully developed flow without control. When the control was turn on, the skin friction coefficient, $C_f = (1/2)\rho U_b^2/\tau_w$, rapidly decreased and then relaxed toward a quasi-steady state, as shown in Figure 3. The trend is quite similar to that observed in the DNS of channel flow using the same control algorithm. Statistics shown below were obtained from the data accumulated over approximately 2000 wall unit time-span after the flow was judged to be in a quasi-steady state.

The time traces of control power input density, $[\overline{(p_w/\rho + \frac{1}{2}v_w)v_w}]^+$, for different detection plane locations are shown in Figure 4. It can be noticed that the power input first decreases from $y_d^+ = 5$ to $y_d^+ = 10$ then drastically increases as y_d^+ is increased.

Figure 5 summarizes the relationship between y_d^+ and the drag reduction rate, $R_D = (C_{f0} - C_f)/C_{f0}$, where C_{f0} is the skin friction coefficient of the uncontrolled flow. Corresponding data for channel flow reported by Choi et al. (1994) are also plotted. The dependency of R_D on y_d^+ is similar to that in the channel flow. The maximum drag reduction is attained at $y_d^+ = 15$ for both Reynolds numbers presently specified. The magnitude of drag reduction rate is also comparable to that in the channel despite that the surface area per volume of a pipe is twice as large as that of a channel.

The power saving ratio (or gain), G, is defined as

$$G = \frac{W_{p0} - W_p}{W_a} = \frac{\pi R^2 L(-\frac{dP_0}{dz} + \frac{dP}{dz})U_b}{2\pi RL\overline{(p_w + \frac{1}{2}\rho v_w^2)v_w}}, \tag{2}$$

where p_w is the pressure fluctuation at the wall, while $-dP_0/dz$ and $-dP/dz$ are the mean pressure gradients of uncontrolled and controlled flow, respectively. For channel flow, there is some discrepancy

regarding the value of G among different computations under the same condition. Choi et al. (1994) reported at $Re_b = 3070$ ($Re_{\tau u} \simeq 110$) that the gain was about 30 in the case when the maximum drag reduction rate is achieved with $y_d^+ = 10$. On the other hand, the recent study by Iwamoto et al. (2002) reports $G = 241$ at $Re_b = 3070$ and $G = 167$ at $Re_b = 4600$ ($Re_{\tau u} \simeq 150$) with $y_d^+ = 10$. In the present computation of pipe flow, the gain with the same detection plane location is closer to the channel flow computation by Iwamoto et al. (2002) for both Reynolds numbers, as shown in Figure 6. When $Re_b = 5300$, however, it is much smaller with y_d^+ beyond 10. This is consistent with the increasing power input for larger y_d^+ as already observed in Figure 4.

From the practical point of view, it is of great importance to investigate the net power saving achieved by an active feedback control system. To do this, one should assume the efficiency of the hardware components. In the present study, a total efficiency, η, is defined as

$$\eta = W_a/(W_a + Q_a + Q_s + Q_c)\ , \tag{3}$$

where Q_a, Q_s and Q_c denote the power dissipation in actuators, sensors and controllers, respectively. Figure 7 shows the sum of power input required to drive the flow and that needed to operate the active feedback control system, i.e.,

$$W_{tot} = W_p + (W_a + Q_a + Q_s + Q_c) = \pi R^2 L \left(-\frac{dP}{dz}\right) U_b + \frac{2\pi R L_c \overline{(p_w + \frac{1}{2}\rho v_w^2) v_w}}{\eta} \tag{4}$$

These curves have been normalized by the driving power for uncontrolled flow, W_{p0}, and plotted as functions of y_d^+ for different values of η. It is, of course, natural that the rate of net power saving becomes poorer with the decrease of η. Especially, for both $Re_b = 3050$ and $Re_b = 5300$ cases, one cannot secure net power saving with $\eta < 0.01$ (i.e. less than 1 % efficiency) regardless of the choice of y_d^+. This seems to be a quite severe criterion for a real system, in which, for example, electromagnetic actuators of relatively high power dissipation are used. At $Re_b = 5300$, the maximum net power saving is achieved when the detection plane of $y_d^+ = 10$ is chosen, although the maximum drag reduction is obtained with $y_d^+ = 15$. This is clearly due to very small gain with $y_d^+ = 15$ as shown in Figure 6.

Fundamental statistics of velocity and pressure such as the first and second moments are also accumulated. Although not shown here, changes in these statistics due to control are found to be similar to those in the channel flow.

CONTROL ON PARTIAL WALL

Simulation is continued with control applied only in the region of $0 < z < L_c$ as shown in Figure 8. Hereafter, only the case of $Re_b = 5300$ is considered and the detection plane is fixed at $y_d^+ = 10$. The separation length, L_s, is identical to the computational domain length, i.e. $L_s^+ = L^+ = 7360$.

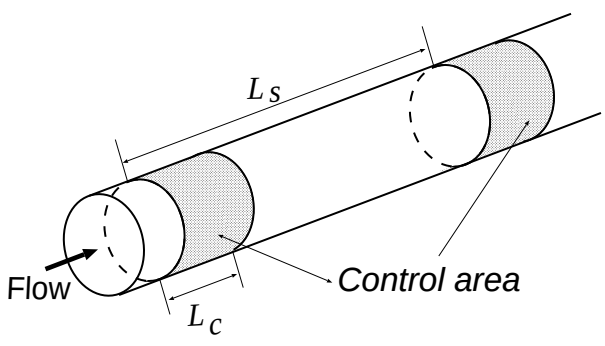

Figure 8: Schematic of partial control.

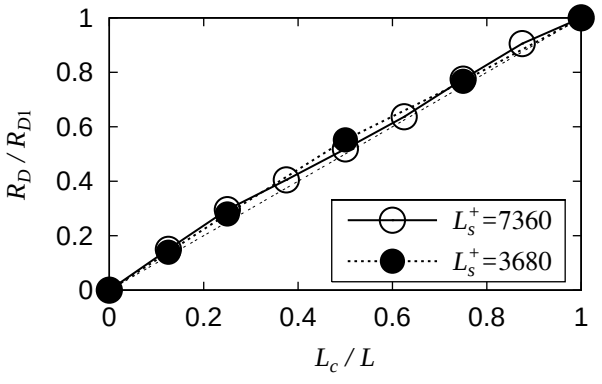

Figure 9: Drag reduction rate as a function of control length.

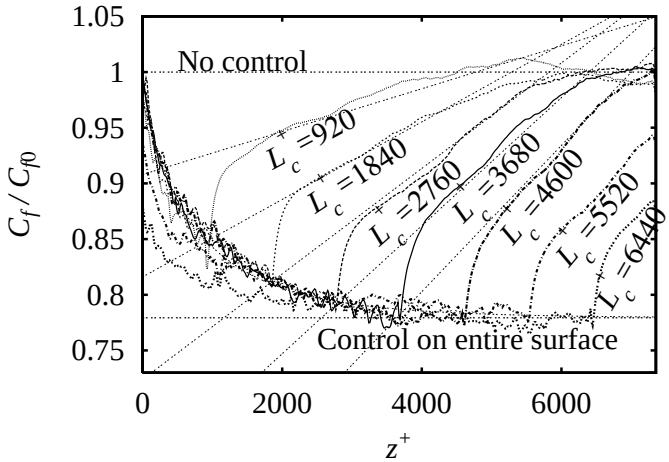

Figure 10: Normalized local skin friction coefficient, for different control length.

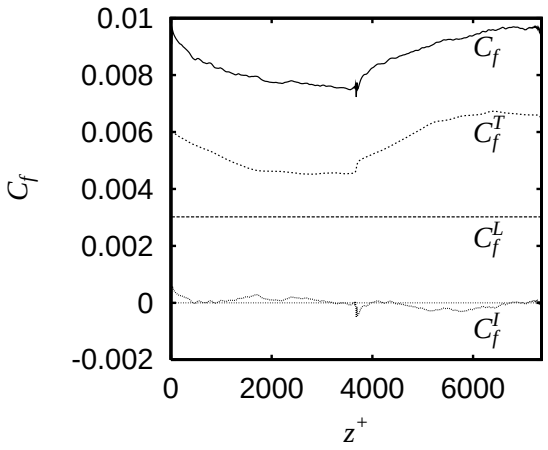

Figure 11: Componential contributions to $C_f(z)$ ($L_z^+ = 3680$).

Figure 9 [2] shows the drag reduction rate, R_D, as a function of L_c^+. Computed reduction rate is nearly proportional to the ratio of control length to separation length, i.e., $R_D \simeq (L_c/L_s)R_{D1}$, where R_{D1} is the drag reduction rate with control on entire wall.

This result can be explained by the behavior of the local skin friction coefficient, $C_f(z)$, plotted in Figure 10[2]. The common behavior observed regardless of the value of L_c is as follows. In the controlled region, $C_f(z)$ decreases following a single curve which may be curve-fitted as $(C_f(z)/C_{f0}) = (C_{f1}/C_{f0}) + [1-(C_{f1}/C_{f0})\exp\{-(z^+/L_a^+)^b\}]$, where C_{f1} denotes the skin friction coefficient with control on the entire wall. A least square fit gives $L_a^+ = 745 \pm 7$ and $b = 0.76 \pm 0.01$. Just after the control ends, say in the region of $L_c^+ < z^+ < L_c^+ + 60$, the skin friction rapidly increases. Subsequently, C_f increases almost linearly up to the level of the uncontrolled flow. This linear line can be expressed as $(C_f(z)/C_{f0}) = cz^+ + d$. The coefficients of c and d can also be obtained from fitting, though at the same time they should be determined to be consistent in the $L_c \to \infty$ limit. The results are $c = c_\infty[1-\exp(-L_c^+/4000)]$ and $d = 1 - c_\infty L_c^+$ with $c_\infty = 1\times10^{-4}$. The lines of this model are also drawn in Figure 10. By using the modeled curve, the endurance length of control effect after the end point of control in the $L_c \to \infty$ limit can be estimated as $R_{D1}/c_\infty \simeq 2200$.

Although not shown here, some cases are also computed with a shorter separation length, i.e., $L_s^+ = 3800$. The trend in the local skin friction coefficient is similar to that presented above. In the case where the length of uncontrolled region is shorter than endurance length, e.g., $L_c^+ = 2850$, the skin friction coefficient does not recover to the level of uncontrolled flow and C_f in the control region deviates from the modeled curve. Even in such case, the drag reduction rate is found to be nearly proportional to the ratio of L_c/L_s.

For the present flow condition, the relation between the local skin friction coefficient and the other statistical quantities can be expressed as

$$C_f(z) = \underbrace{\frac{16}{Re_b}}_{C_f^L} + \underbrace{64\int_0^1\left[\int_r^1 \overline{u_r'u_z'}dr\right]rdr}_{C_f^T} + \underbrace{64\int_0^1\left[\int_r^1 \overline{u_r}\,\overline{u_z}dr\right]rdr + 64\int_0^1\left[\int_r^1\left\{\int_0^r\left(\frac{\partial u_z u_z}{\partial z} - \frac{1}{Re_b}\frac{\partial^2 u_z}{\partial z^2} + \frac{\partial p}{\partial z}\right)'' rdr\right\}dr\right]rdr}_{C_f^I}, \quad (5)$$

[2] Additional data points has been added to the published version.

where $\bar{\cdot}$ and $\cdot'$ denote the average and fluctuations based on the averaging in the homogeneous directions (viz., the averaged quantity is a function of r and z), whereas the double-prime ($\cdot''$) represents a deviation of that average ($\bar{\cdot}$) from the local bulk mean (see, Appendix for the derivation and detailed definitions on averaging). Namely, $C_f(z)$ can be decomposed into contributions from three effects:

1. laminar effect, C_f^L,
2. turbulent effect, C_f^T,
3. effect of the statistical inhomogeneity in the streamwise direction, C_f^I.

Figure 11 shows the magnitudes of these effects computed in the case of $L_c^+ = 3680$. Here, the contributions of C_f^T and C_f^L are dominant and the inhomogeneity effect is very small. Therefore, the cause for rapid increase of $C_f(z)$ should be studied by examining the Reynolds shear stress, $\overline{u_r' u_z'}$.

The source and sink terms in the budget of Reynolds shear stress $\overline{u_r' u_z'}$ are,

$$P_{rz}^+(r^+, z^+) = -\overline{u_r'^+ u_r'^+} U_{z,r}^+ - \overline{u_z'^+ u_z'^+} U_{r,z}^+ , \tag{6}$$

$$\phi_{rz}^+(r^+, z^+) = \overline{p'^+ (u_{r,z}'^+ + u_{z,r}'^+)} , \tag{7}$$

where Eqs. (6) and (7) are the production term and the pressure-strain term, respectively. Figures 12 and 13 show the contours of these terms around the end point of control in the case of $L_c^+ = 3680$. As is seen in Figure 12, the production is significantly suppressed in the upstream control region as compared to that of the uncontrolled flow, which reached $P_{rz}^+ \simeq 0.07$ at $y^+ = 20$. After the control region ends, P_{rz}^+ increases in the whole cross section. The rate of increase, however, does not seem to be large enough to be responsible for the rapid increase of C_f.

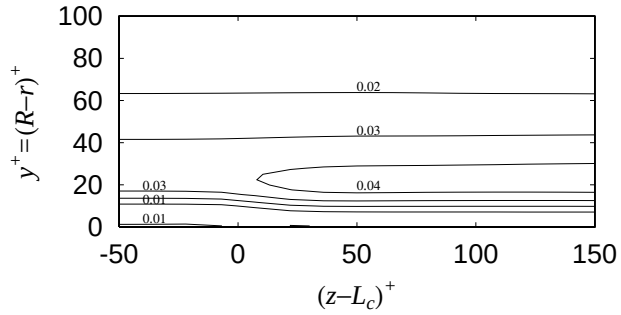

Figure 12: Production term in ($\overline{u_r' u_z'}$) budget ($L_c^+ = 3680$).

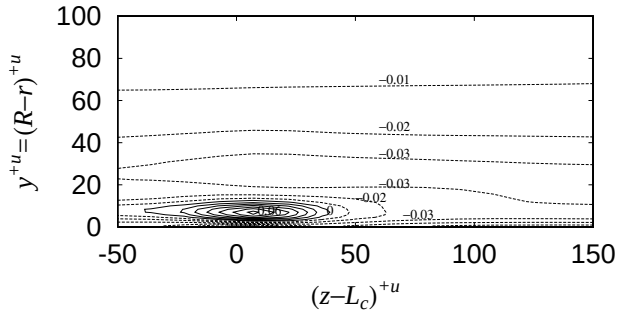

Figure 13: Pressure-strain term in ($\overline{u_r' u_z'}$) budget ($L_c^+ = 3680$).

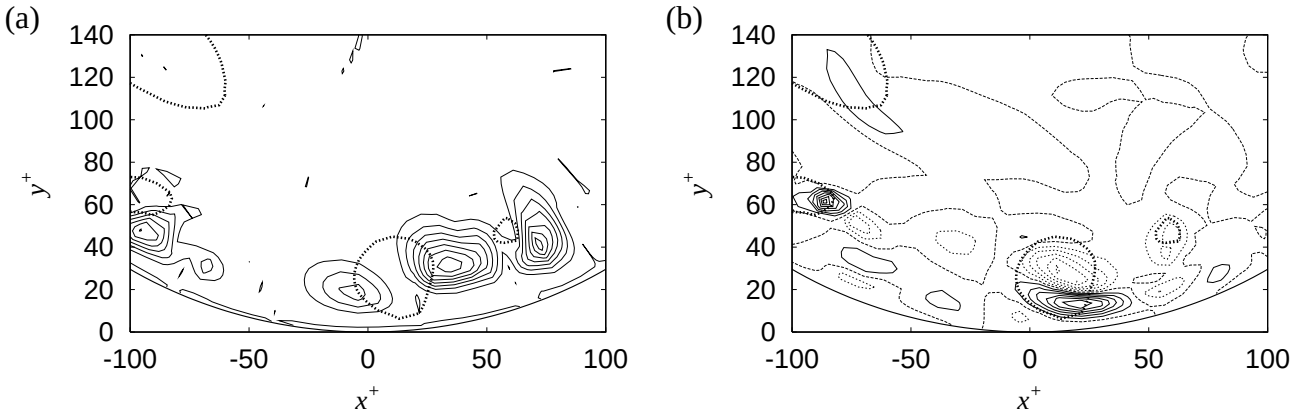

Figure 14: Contours in a cross stream plane at $(z - L_c)^+ = 7$. (a) Production term (increment is 0.05); (b) Pressure-strain term (increment is 0.2).

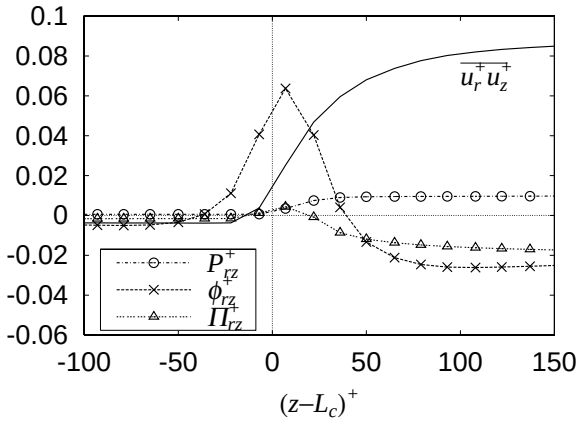

Figure 15: Streamwise profile of production, P_{rz}, pressure-strain, ϕ_{rz}^+, and velocity-pressure gradient, Π_{rz}^+, at $y^+ = 7$.

Anomalous behavior can rather be observed in ϕ_{rz}^+. In most of the domain in Figure 13, the contour levels are quite similar to that of the uncontrolled flow and therefore ϕ_{rz} works as a sink. However, one can clearly observe a region with strong positive value of ϕ_{rz}^+ around the endpoint of control. This region has a size of 10 and 80 wall units in the wall-normal (radial) and streamwise directions, respectively. At the center of this region, $y^+ = 7$, $(z-L_c)^+ = 7$, the value of ϕ_{rz}^+ increases up to 0.06, which is comparable to the maximum value of P_{rz}^+ in the uncontrolled flow.

Contours of P_{rz}^+ and ϕ_{rz}^+ in an instantaneous field in the $r-theta$ cross-section at $(z-L_c)^+ = 7$ are shown in Figure 14 together with supplemental contours of local pressure. The thin lines are contours of P_{rz}^+ and ϕ_{rz}^+ (solid line, positive; dashed line, zero; dotted line, negative) and the thick lines are iso-lines of pressure fluctuation (solid line, $p'^+ = 2.0$, not observed in the presented area; dotted line, $p'^+ = -2.0$). Like in uncontrolled channel flow (Kasagi et al., 1995), P_{rz}^+ has large values next to the vortex core that can be found, e.g., around $(x,\ y) = (10,\ 30)$. The relative location between the vortex and the high production regions with respect to the direction of rotation, which was examined by the sign of local vorticity, is also the same. However, neither the high pressure region that should be found somewhere up-left of that vortex or the near-wall high pressure region cannot be found in this case, and this fact may imply that the motion of this vortex is rather weak.

The distribution of pressure-strain is also similar to that of uncontrolled channel flow. However, the peak value in the positive region just below the vortex is very high and is about $\phi_{rz}^+ = 1.5$. Considering that ϕ_{rz}^+ is extremely small in other region, it is plausible that such high positive peak causes the positive mean value of ϕ_{rz}^+.

Figure 15 shows the streamwise distribution of the production, P_{rz}^+, pressure-strain, ϕ_{rz}^+, and velocity-pressure gradient, Π_{rz}, at $y^+ = 7$. For comparison, the corresponding profile of the Reynolds shear stress $\overline{u_r' u_z'}$ is also plotted. It is found that the explosive increase of pressure-strain term is canceled by the pressure-diffusion. However, Π_{rz}^+ is still weakly positive until $(z-L_z)^+ \simeq 20$ and it helps the rapid increase of C_f even under the small production.

CONCLUSIONS

Active cancellation control was applied to DNS of turbulent pipe flow. From the simulation with control on the entire surface, we found:

1. The maximum drag reduction rate is comparable to that of channel flow (~ 25 %);
2. At least, a total device efficiency more than 1 % is required for a real active feedback control system to attain net power saving.

From the simulation with control on partial surface, the following results were obtained:

1. Even if the control is not applied on an entire surface, the drag reduction proportional to the area of control (or slightly larger effect than that) can be obtained;
2. The flow recovers to the uncontrolled state about $2000-2500$ wall unit length downstream of the end point of control;
3. The rapid increase of the skin friction is observed soon after the end point of control and it is seemingly caused by weak (or slightly positive) velocity-pressure gradient correlation.

As is suggested by the present results, a still higher drag reduction rate can be expected by the partial control if one can avoid the rapid recovery of Reynolds shear stress soon after the end point of control. This may be made possible by modifying the control algorithm based on further investigation on the dynamics there, although such work is left for the future.

ACKNOWLEDGMENT

This work was supported through the Project for Organized Research Combination System by the Ministry of Education, Culture, Sports and Technology of Japan (MEXT).

APPENDIX: DERIVATION OF EQ. (5)

At first, we derive the relation between local friction coefficient, $C_f(z)$ and local mean pressure gradient, $(-\widetilde{\overline{\partial p/\partial z}})(z)$, in the case where flow is inhomogeneous in the z direction. Here, $\widetilde{\cdot}$ denotes the local bulk mean, i.e., the average in r-θ plane. The momentum equation in the z direction can be nondimensionalized by ρ, R and $2U_b$ as:

$$\frac{\partial u_z}{\partial t} = -\frac{1}{r}\frac{\partial}{\partial r}(ru_ru_z) - \frac{1}{r}\frac{\partial}{\partial \theta}(u_\theta u_z) - \frac{\partial}{\partial z}(u_z u_z) - \frac{\partial p}{\partial z} + \frac{1}{Re_b}\left(\frac{1}{r}\frac{\partial}{\partial r}r\frac{\partial u_z}{\partial r} + \frac{1}{r}\frac{\partial^2 u_z}{\partial \theta^2} + \frac{\partial^2 u_z}{\partial z}\right) . \tag{8}$$

Under the condition of constant mass flow rate and blowing / suction condition at walls, i.e., $u_r \neq 0$ and $u_z = u_\theta = 0$, an integration of Eq. (8) in $r-\theta$ plane can be reduced to read

$$\begin{aligned} -\widetilde{\overline{\frac{\partial p}{\partial z}}}(z) &= -\frac{2}{Re_b}\frac{\partial \widetilde{\overline{u_z}}}{\partial r} + \frac{\partial \widetilde{\overline{u_z u_z}}}{\partial z} - \frac{1}{Re_b}\frac{\partial^2 \widetilde{\overline{u_z}}}{\partial z^2} \\ &= \frac{1}{4}C_f(z) + \widetilde{\overline{a}}(z) , \end{aligned} \tag{9}$$

where a is defined as

$$a = \frac{\partial u_z u_z}{\partial z} - \frac{1}{Re_b}\frac{\partial^2 u_z}{\partial z^2} . \tag{10}$$

On the other hand, the average of Eq. (8) in the homogeneous directions, i.e. θ and time, yields

$$-\frac{\partial \overline{p}}{\partial z}(r,z) = \frac{1}{r}\frac{\partial}{\partial r}r\left[\overline{u_r}\,\overline{u_z} + \overline{u_r' u_z'} - \frac{1}{Re_b}\frac{\partial \overline{u_z}}{\partial r}\right] + \overline{a}(r,z) , \tag{11}$$

where $u_z(r,\theta,z,t) = \overline{u_z}(r,z) + u_z'(r,\theta,z,t)$. This can be formally split as

$$-\widetilde{\overline{\frac{\partial p}{\partial z}}} - \frac{\partial p''}{\partial z} = \frac{1}{r}\frac{\partial}{\partial r}r\left[\overline{u_r}\,\overline{u_z} + \overline{u_r' u_z'} - \frac{1}{Re_b}\frac{\partial \overline{u_z}}{\partial r}\right] + \overline{a}(r,z) , \tag{12}$$

where $\overline{p}(r,z) = \widetilde{\overline{p}}(z) + p''(r,z)$.

Substitution of Eq. (9) into Eq. (12) yields

$$\frac{1}{4}C_f(z) = \frac{1}{r}\frac{\partial}{\partial r}r\left[\overline{u_r}\,\overline{u_z} + \overline{u_r' u_z'} - \frac{1}{Re_b}\frac{\partial \overline{u_z}}{\partial r}\right] + a''(r,z) + \frac{\partial p''}{\partial z}(r,z)\,. \tag{13}$$

Finally, by applying a triple integration, i.e., $\int_0^1 r dr \int_r^1 dr \int_0^r r dr$, we obtain Eq. (5).

Note that, in the cases where the flow is homogeneous in the z direction, the third term of Eq. (5) is zero and the expression becomes similar to that used by Iwamoto et al. (2002).

REFERENCES

Choi H., Moin P. and Kim J. (1994). Active turbulence control for drag reduction in wall bounded flows. *J. Fluid Mech.* **262**, 75-110.

Eggels J.G.M., Unger F., Weiss M.H., Westerweel J., Adrian R.J., Friedrich R. and Nieuwstadt F.T.M. (1994). Fully developed turbulent pipe flow: a comparison between direct numerical simulation and experiment. *J. Fluid Mech.* **268**, 175-209.

Endo T., Kasagi N. and Suzuki, Y. (2000). Feedback control of wall turbulence with wall deformation. *Int. J. Heat Fluid Flow* **21**, 568-575.

Fukagata K. and Kasagi N. (2002). Highly energy-conservative finite difference method for cylindrical coordinate system. *J. Comput. Phys.* **181**, 478-498.

Iwamoto K., Suzuki Y. and Kasagi N. (2002). Reynolds number effect on wall turbulence: Toward effective feedback control. *Int. J. Heat Fluid Flow* **23**, 678-689.

Kasagi N., Sumitani Y., Suzuki Y. and Iida O. (1995). Kinematics of the quasi-coherent vortical structure in near-wall turbulence. *Int. J. Heat Fluid Flow* **16**, 2-10.

Lee C., Kim J. and Choi H. (1998). Suboptimal control of turbulent channel flow for drag reduction. *J. Fluid Mech.* **358**, 245-258.

Orlandi P. and Fatica M. (1997). Direct simulations of turbulent flow in a pipe rotating about its axis. *J. Fluid Mech.*, **343**, 43-72.

Quadrio M. and Sibilla S. (2000). Numerical simulation of turbulent flow in a pipe oscillating around axis. *J. Fluid Mech.*, **424**, 217-241.

Rai M.M. and Moin P. (1991). Direct numerical simulations of turbulent flow using finite difference schemes. *J. Comput. Phys.* **96**, 15-53.

You J., Choi H. and Yoo J.Y. (2000). A modified fractional step method of keeping a constant mass flow rate in fully developed channel and pipe flows. *KSME Int. J.* **14**, 547-552.